

One-sided Stability of MAT and Its Applications

Sung Woo Choi and Hans-Peter Seidel

Computer Graphics Group
Max-Planck-Institut für Informatik
Stuhlsatzenhausweg 85, 66123 Saarbrücken, Germany
Email: {swchoi, hpseidel}@mpi-sb.mpg.de

Abstract

Although useful in many applications, the medial axis transform (MAT) has a few fit-falls, one of which is its extreme sensitivity to the boundary perturbation. In this paper, we first summarize the previous attempts to get around this by bounding the one-sided Hausdorff distance of the MAT with respect to the boundary perturbation. We illustrate these results and their optimality with various examples. Finally, we suggest an application of them in pruning. In particular, we discuss the advantage of the results for the domains which are not weakly injective, over those for the weakly injective ones.

1 Introduction

The *medial axis* (MA), sometimes called the skeleton, or the symmetric axis, was first introduced by Blum [4]. It is defined as the set of the centers of the maximal inscribed circles contained in the given domain. The *medial axis transform* (MAT), which incorporates the radius information important for the reconstruction of the original domain, is defined as the set of all the pairs of the medial axis point and the radius of the corresponding inscribed circle. Explicitly, the medial axis transform $\mathbf{MAT}(\Omega)$ and the medial axis $\mathbf{MA}(\Omega)$ of a plane domain Ω is defined by

$$\begin{aligned}\mathbf{MAT}(\Omega) &= \{(p, r) \in \mathbb{R}^2 \times [0, \infty) \mid \\ &\quad B_r(p) \text{ is a maximal ball in } \Omega\}, \\ \mathbf{MA}(\Omega) &= \{p \in \mathbb{R}^2 \mid \exists r \geq 0, \\ &\quad \text{s.t. } (p, r) \in \mathbf{MAT}(\Omega)\}.\end{aligned}$$

Having a natural definition, the medial axis transform has a graph structure which preserves the original shape homotopically [3, 4, 5]. So it has been

one of the most widely-used tools in shape analysis. But the medial axis transform is very sensitive to the boundary perturbation [1, 2, 7, 12, 15, 16]. For example, even if we perturb only slightly the boundary of the domain in (a) of Figure 1, the resulting changes in MA and MAT are big, that is, the two-sided Hausdorff distances between these MA's and MAT's are large. See the domain in (b) of Figure 1.

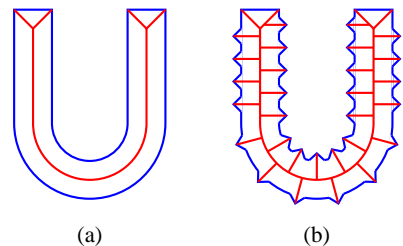


Figure 1: Sensitivity of MAT to the boundary perturbation: Infinitesimally small perturbation of the boundary can result in a drastic change in MAT. But the one-sided Hausdorff distance still remains stable.

On the other hand, it can be observed that the MA and MAT in (a) are approximately contained in those in (b) of Figure 1. So the *one-sided* Hausdorff distances of MA and MAT in (a) with respect to those in (b) still remain small, as long as the perturbation is small.

These phenomenon was first quantified for a special class of the domains called the *injective domains* in [7], and has been generalized in [9, 10]. We will review these results, and give an application of them in the pruning of the medial axis transform [11, 14, 17].

An important feature of this application is that

we can calculate *a priori* error bound of the pruning only by examining the boundary curves of the approximating domain. It also provides a theoretical basis for handling the medial axis transform in the multi-resolution manner.

2 Hierarchy of Domains

The following is a general assumption on the domains we consider:

- Ω is compact, or equivalently, Ω is closed and bounded.
- The boundary $\partial\Omega$ of Ω is a (disjoint) union of finitely many simple closed curves, each of which in turn consists of finitely many real-analytic curve pieces.

We will call the domains with the above condition *normal*. This assumption is optimal [5] in the sense that it is both general enough and necessary to guarantee the reasonable behaviour of **MAT**.

We call an end point of **MA** (or **MAT**) a *1-prong point*. There are exactly three kinds of the 1-prong points in **MA**, which are depicted in Figure 2; Type (a) is the center of a maximal circle with only one contact point at which the circle osculates the boundary. Type (b) is a sharp corner. Type (c) is a 1-prong point with a contact arc. We call a 1-prong point of the type (a) a *non-degenerate 1-prong point*.

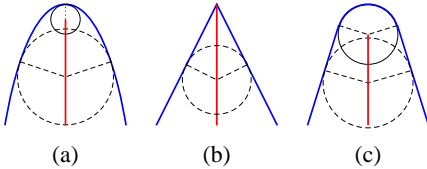


Figure 2: Three types of 1-prong points

We call a normal domain Ω *injective*, if every 1-prong point of **MAT**(Ω) is of the type (c), and *weakly injective*, if **MAT**(Ω) has no non-degenerate 1-prong points, *i.e.*, the 1-prong points of the type (a). So we have the following inclusion relations:

$$\begin{aligned} &\{\text{injective domains}\} \\ &\quad \cap \\ &\{\text{weakly injective domains}\} \\ &\quad \cap \\ &\{\text{normal domains}\} \end{aligned}$$

For more details on the properties of the medial axis transform, see [3, 4, 5].

3 Hausdorff Distances

The (*two-sided*) Hausdorff distance between A and B , $\mathcal{H}(A, B)$, is defined by

$$\mathcal{H}(A, B) = \max \{ \mathcal{H}(A|B), \mathcal{H}(B|A) \},$$

for any two (compact) sets A and B in \mathbb{R}^n , $n = 1, 2, \dots$, where, $\mathcal{H}(A|B)$, the *one-sided Hausdorff distance* of A with respect to B is defined by

$$\mathcal{H}(A|B) = \max_{p \in A} d(p, B).$$

Here $d(\cdot, \cdot)$ is the usual Euclidean distance. While the two-sided Hausdorff distance measures the difference between two sets, the one-sided Hausdorff distance measures how approximately one set is contained in another set.

In showing the bounds in the following sections, it is crucial to use the *hyperbolic Hausdorff distance*, which was introduced in [8]. Denote $\mathbb{R}_{\geq 0} = \{x \in \mathbb{R} \mid x \geq 0\}$. For two compact sets M_1, M_2 in $\mathbb{R}^2 \times \mathbb{R}_{\geq 0}$, the (*two-sided*) hyperbolic Hausdorff distance between M_1 and M_2 is defined by

$$\begin{aligned} \mathcal{H}_h(M_1, M_2) \\ = \max \{ \mathcal{H}_h(M_1|M_2), \mathcal{H}_h(M_2|M_1) \}, \end{aligned}$$

where

$$\mathcal{H}_h(M_1|M_2) = \max_{P_1 \in M_1} \left\{ \min_{P_2 \in M_2} d_h(P_1|P_2) \right\}.$$

Here,

$$d_h(P_1|P_2) = \max \{ 0, d(p_1, p_2) - (r_2 - r_1) \},$$

for $P_1 = (p_1, r_1), P_2 = (p_2, r_2)$ in $\mathbb{R}^2 \times \mathbb{R}_{\geq 0}$.

The hyperbolic Hausdorff distance is a metric especially adapted to the medial axis transform. We mention that a similar, but different metric is proposed in [6].

4 Bounds for Injective and Weakly Injective Domain

Let Ω be a normal domain. Except for some finite number of the special points, the maximal ball

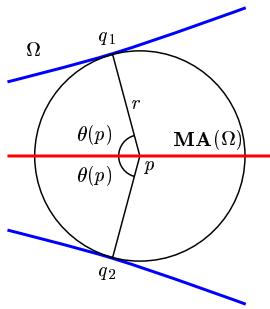


Figure 3: Generic point in MA of a normal domain

$B_r(p)$ for every $P = (p, r) \in \mathbf{MAT}(\Omega)$, has exactly two contact points with the boundary $\partial\Omega$, and $\mathbf{MA}(\Omega)$ is a C^1 curve around such p in \mathbb{R}^2 . See Figure 3.

We denote the set of all such *generic* points in $\mathbf{MA}(\Omega)$ by $G(\Omega)$, and, for every $p \in G(\Omega)$, define $0 < \theta(p) \leq \frac{\pi}{2}$ to be the angle between $\overline{pq_1}$ (or equivalently, $\overline{pq_2}$) and $\mathbf{MA}(\Omega)$ at p , where q_1, q_2 are the two contact points.

Now, for every normal domain Ω , we define

$$\begin{aligned} \theta_\Omega &= \inf \{ \theta(p) : p \in G(\Omega) \}, \\ \rho_\Omega &= \min \{ r : (p, r) \in \mathbf{MAT}(\Omega) \}. \end{aligned}$$

Note that $0 \leq \theta_\Omega \leq \frac{\pi}{2}$, and ρ_Ω is the smallest radius of the maximal balls contained in Ω .

It is easy to see that $\theta_\Omega = 0$, if and only if $\mathbf{MA}(\Omega)$ has a 1-prong point of the type (a), and $\rho_\Omega = 0$, if and only if $\mathbf{MA}(\Omega)$ has a 1-prong point of the type (b). Thus, Ω is injective, if and only if $\rho_\Omega > 0$ and $\theta_\Omega > 0$, and it is weakly injective, if and only if $\theta_\Omega > 0$. Note that a weakly injective domain may have a sharp corner (*i.e.*, the type (b)), while an injective domain may not.

For injective and weakly injective domains, the one-sided Hausdorff distance of MA and MAT are bounded linearly by the magnitude of the perturbation in the following ways:

Proposition 1. (One-sided Stability for Injective Domain) [7, 9]

Let Ω be an injective domain. Then we have

$$\begin{aligned} \mathcal{H}(\mathbf{MA}(\Omega) | \mathbf{MA}(\Omega')) &\leq \frac{2}{1 - \cos \theta_\Omega} \cdot \epsilon + o(\epsilon), \\ \mathcal{H}(\mathbf{MAT}(\Omega) | \mathbf{MAT}(\Omega')) &\leq \frac{\sqrt{4 + (3 - \cos \theta_\Omega)^2}}{1 - \cos \theta_\Omega} \cdot \epsilon + o(\epsilon), \end{aligned}$$

for every normal domain Ω' such that $\max \{ \mathcal{H}(\Omega, \Omega'), \mathcal{H}(\partial\Omega, \partial\Omega') \} \leq \epsilon$.

For $\theta \in (0, \pi/2]$, let

$$g(\theta) = 3 \left(1 + \frac{2\sqrt{1 + \cos^2 \theta}}{1 - \cos \theta} \right).$$

Proposition 2. (One-sided Stability for Weakly Injective Domain) [9]

Let Ω be a weakly injective domain. Then we have

$$\begin{aligned} \mathcal{H}(\mathbf{MAT}(\Omega) | \mathbf{MAT}(\Omega')) &\leq g(\theta_\Omega) \cdot \epsilon + o(\epsilon), \\ \mathcal{H}(\mathbf{MA}(\Omega) | \mathbf{MA}(\Omega')) &\leq g(\theta_\Omega) \cdot \epsilon + o(\epsilon), \end{aligned}$$

for every normal domain Ω' such that $\max \{ \mathcal{H}(\Omega, \Omega'), \mathcal{H}(\partial\Omega, \partial\Omega') \} \leq \epsilon$.

5 Bound for Normal Domain

Now we consider the normal domains which are not weakly injective. We first classify the non-degenerate 1-prong points into the three types. See Figure 4.

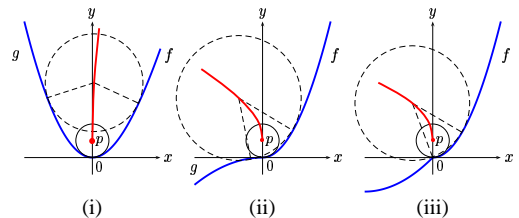


Figure 4: Three types of non-degenerate 1-prong points

Suppose $P = (p, r)$ is a non-degenerate 1-prong point of $\mathbf{MAT}(\Omega)$, and let $q \in \partial\Omega$ be its contact point. With an appropriate rigid motion in the plane, we can assume that $q = (0, 0)$ and $p = (0, r)$. We

can also assume that for small $\delta > 0$, there is a function $f : [0, \delta] \rightarrow \mathbb{R}$,

$$f(x) = \sum_{n=2}^{\infty} a_n x^n,$$

such that the graph of f is on $\partial\Omega$. Note that $a_2 = \frac{k}{2}$, where $k = k_P = \frac{1}{r}$. When $\partial\Omega$ is not C^1 at q , we call P of type (iii) (See Figure 4 (iii)). Suppose $\partial\Omega$ is C^1 at q . Then we can take a function $g : [-\delta, 0] \rightarrow \mathbb{R}$,

$$g(x) = \sum_{n=2}^{\infty} b_n x^n,$$

such that the graph of g is on $\partial\Omega$. We call P of the type (i) (resp., of the type (ii)), if $b_2 = \frac{k}{2}$ (resp., $b_2 \neq \frac{k}{2}$), that is, if $\partial\Omega$ is C^2 (resp., not C^2) at q . See Figure 4 (i), (ii). We assume with no loss of generality that $f(t) \leq g(-t)$ (resp., $f(t) \geq g(-t)$) for $t \in [0, \delta]$, in the case of the type (i) (resp., of the type (ii)). So we have $b_2 < \frac{k}{2}$ in the case of the type (ii).

Define the arc function \mathcal{A}_k as follows:

$$\begin{aligned} \mathcal{A}_k(x) &= \frac{1}{k} - \frac{1}{k} \sqrt{1 - k^2 x^2} \\ &= \frac{1}{2} k x^2 + \frac{1}{8} k^3 x^4 + \frac{1}{16} k^5 x^6 + \dots \\ &=: \sum_{n=2}^{\infty} k^{n-1} Q_n x^n. \end{aligned} \tag{1}$$

The graph of \mathcal{A}_k is the lower half of the circle with the radius $r = \frac{1}{k}$ with the center $(0, r) = (0, \frac{1}{k})$. See Figure 5.

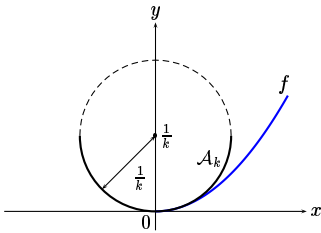


Figure 5: The arc function and the boundary

For each $n = 2, 3, \dots$, let A_n be the difference of the coefficient of the n -th term of \mathcal{A}_k with respect to that of f , i.e., $A_n = k^{n-1} Q_n - a_n$. Denote by

N_P the largest integer such that $A_2 = A_3 = \dots = A_{N_P} = 0$. Note that we always have $N_P \geq 2$ and $A_{N_P+1} > 0$. Let

$$N_\Omega = \min \{N_P : P \text{ is a non-degenerate 1-prong of } \mathbf{MAT}(\Omega)\}.$$

For each non-degenerate 1-prong point P of $\mathbf{MAT}(\Omega)$, we define

$$K_P = \frac{\sqrt{2} \cdot 12^{\frac{N_P-1}{N_P+1}} (N_P + 1)}{k_P^2 (N_P - 1)^{\frac{N_P-1}{N_P+1}}} \cdot A_{N_P+1}^{\frac{2}{N_P+1}},$$

if P is of the type (i), and

$$K_P = \frac{\sqrt{2} \cdot 2^{\frac{3N_P-1}{N_P+1}} \cdot 6^{\frac{N_P-1}{N_P+1}} \cdot N_P^{\frac{2N_P}{N_P+1}}}{k_P^2 (N_P - 1)^{\frac{2(N_P-1)}{N_P+1}}} \cdot A_{N_P+1}^{\frac{2}{N_P+1}},$$

if P is of the type (ii).

Suppose that every non-degenerate 1-prong point of $\mathbf{MAT}(\Omega)$ is of the type (i) or (ii). We let

$$K_\Omega = \max \{K_P : P \text{ is a non-degenerate 1-prong point of } \mathbf{MAT}(\Omega) \text{ s.t. } N_P = N_\Omega\}.$$

It is important to note that K_Ω can be calculated directly from $\partial\Omega$.

Proposition 3. [10]

Let Ω be a normal domain which is not weakly injective. Suppose that $\mathbf{MAT}(\Omega)$ has no non-degenerate 1-prong points of the type (iii). Then we have

$$\begin{aligned} \mathcal{H}(\mathbf{MA}(\Omega)|\mathbf{MA}(\Omega')) &\leq K_\Omega \cdot \epsilon^{\frac{N_\Omega-1}{N_\Omega+1}} + o\left(\epsilon^{\frac{N_\Omega-1}{N_\Omega+1}}\right), \\ \mathcal{H}(\mathbf{MAT}(\Omega)|\mathbf{MAT}(\Omega')) &\leq K_\Omega \cdot \epsilon^{\frac{N_\Omega-1}{N_\Omega+1}} + o\left(\epsilon^{\frac{N_\Omega-1}{N_\Omega+1}}\right), \end{aligned}$$

for every normal domain Ω' such that $\max \{\mathcal{H}(\Omega, \Omega'), \mathcal{H}(\partial\Omega, \partial\Omega')\} \leq \epsilon$.

See [10] for the analysis of the case when Ω has a non-degenerate 1-prong point of the type (iii). We mention here that Morse lemma [13] is an important tool for showing the above bounds.

6 Illustrating Examples

Now we illustrate with a few examples the result in the previous section. See [9] for the examples of the weakly injective case.

The following three examples correspond to the type (i) in Figure 4.

Example 1. Let Ω be the domain as depicted in Figure 6, and let Ω' be the domain such that $\mathbf{MAT}(\Omega')$ is obtained after cutting away the portion of $\mathbf{MAT}(\Omega)$ between $P = (p, r)$ and $P' = (p', r')$.

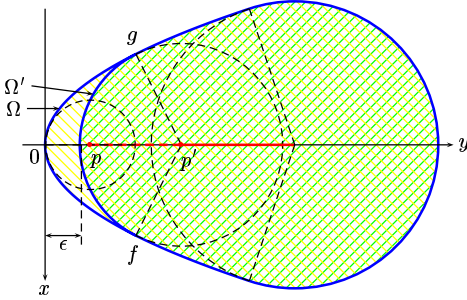


Figure 6: Non-degenerate 1-prong point of the type (i): quadratic case

Here, we let $f(x) = g(x) = \frac{k}{2}x^2$, where $k = k_P = \frac{1}{r}$. From (1), we have $A_3 = 0$, $A_4 = \frac{k^3}{8}$, and $N_P = 3$. In this case, it turns out that

$$\begin{aligned} \mathcal{H}(\mathbf{MA}(\Omega)|\mathbf{MA}(\Omega')) &= \frac{\sqrt{2}}{\sqrt{k}} \cdot \sqrt{\epsilon} + o(\sqrt{\epsilon}), \\ \mathcal{H}(\mathbf{MAT}(\Omega)|\mathbf{MAT}(\Omega')) &= \frac{2}{\sqrt{k}} \cdot \sqrt{\epsilon} + o(\sqrt{\epsilon}), \end{aligned}$$

where $\epsilon = \max\{\mathcal{H}(\Omega, \Omega'), \mathcal{H}(\partial\Omega, \partial\Omega')\} = \mathcal{H}(\partial\Omega, \partial\Omega')$.

Example 2. (Ellipse) Let Ω be the ellipse defined by

$$\frac{x^2}{a^2} + \frac{(y-b)^2}{b^2} = 1,$$

for some $b > a > 0$, and let Ω' be the domain such that $\mathbf{MAT}(\Omega')$ is obtained after cutting away the portion of $\mathbf{MAT}(\Omega)$ between $P = (p, r)$ and $P' = (p', r')$. See Figure 7.

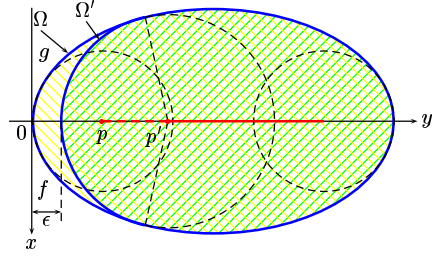


Figure 7: Non-degenerate 1-prong point of the type (i): ellipse

Here, we have $k_P = \frac{1}{r} = \frac{b}{a^2}$, and

$$\begin{aligned} f(x) &= g(x) \\ &= b - b\sqrt{1 - \frac{x^2}{a^2}} \\ &= \frac{b}{2a^2}x^2 + \frac{b}{8a^4}x^4 + \frac{b}{16a^6}x^6 + \dots, \\ \mathcal{A}_{\frac{b}{a^2}}(x) &= \frac{b}{2a^2}x^2 + \frac{b^3}{8a^6}x^4 + \frac{b^5}{16a^{10}}x^6 + \dots. \end{aligned}$$

So we have $A_3 = 0$ and $A_4 = \frac{b}{8a^6}(b^2 - a^2)$, and $N_P = 3$. Let $\epsilon = \max\{\mathcal{H}(\Omega, \Omega'), \mathcal{H}(\partial\Omega, \partial\Omega')\} = \mathcal{H}(\partial\Omega, \partial\Omega')$. In this case, we have

$$\begin{aligned} \mathcal{H}(\mathbf{MA}(\Omega)|\mathbf{MA}(\Omega')) &= \frac{\sqrt{2}a}{b\sqrt{b}}\sqrt{b^2 - a^2} \cdot \sqrt{\epsilon} + o(\sqrt{\epsilon}), \\ \mathcal{H}(\mathbf{MAT}(\Omega)|\mathbf{MAT}(\Omega')) &= \frac{2a}{b\sqrt{b}}\sqrt{b^2 - a^2} \cdot \sqrt{\epsilon} + o(\sqrt{\epsilon}). \end{aligned}$$

Example 3. Let Ω be the domain as depicted in Figure 8, and let Ω' be the domain such that $\mathbf{MAT}(\Omega')$ is obtained after cutting away the portion of $\mathbf{MAT}(\Omega)$ between $P = (p, r)$ and $P' = (p', r')$.

Here, we let

$$f(x) = \frac{1}{2}x^2 - \frac{1}{24}x^3, \quad g(x) = \frac{1}{2}x^2 + \frac{1}{32}x^4.$$

Now we have $k = 1$, and from (1), we have $A_3 =$

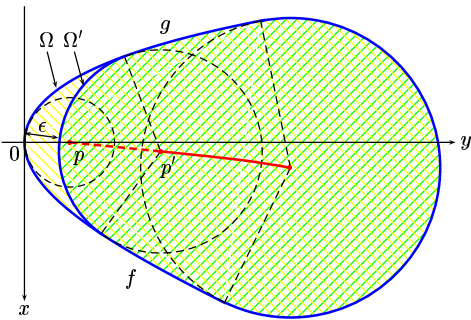


Figure 8: Non-degenerate 1-prong point of the type (i): non-symmetric case

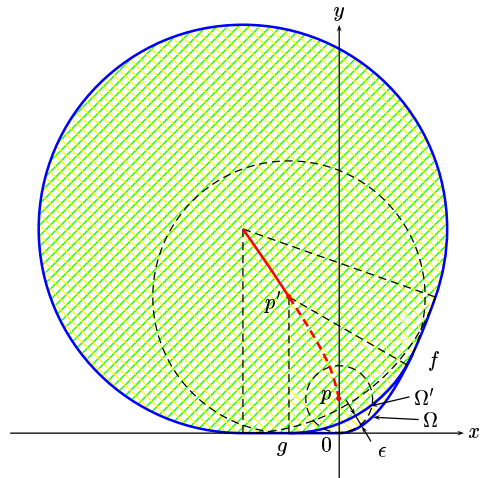


Figure 9: Non-degenerate 1-prong point of the type (ii)

$\frac{1}{24}$, and $N_P = 2$. In this case, it turns out that

$$\begin{aligned} \mathcal{H}(\mathbf{MA}(\Omega)|\mathbf{MA}(\Omega')) &= \sqrt[3]{\frac{3}{32}} \cdot \sqrt[3]{\epsilon} + o(\sqrt[3]{\epsilon}), \\ \mathcal{H}(\mathbf{MAT}(\Omega)|\mathbf{MAT}(\Omega')) &= \sqrt{2} \sqrt[3]{\frac{3}{32}} \cdot \sqrt[3]{\epsilon} + o(\sqrt[3]{\epsilon}), \end{aligned}$$

where $\epsilon = \max \{ \mathcal{H}(\Omega, \Omega'), \mathcal{H}(\partial\Omega, \partial\Omega') \} = \mathcal{H}(\partial\Omega, \partial\Omega')$.

The next example corresponds to the type (ii) in Figure 4.

Example 4. Let Ω be the domain as depicted in Figure 9, and let Ω' be the domain such that $\mathbf{MAT}(\Omega')$ is obtained after cutting away the portion of $\mathbf{MAT}(\Omega)$ between $P = (p, r)$ and $P' = (p', r')$.

Here, we let $f(x) = \frac{k}{2}x^2$, $g(x) = 0$. From (1), we have $A_3 = 0$, $A_4 = \frac{k^3}{8}$, and $N_P = 3$. In this case, it turns out that

$$\begin{aligned} \mathcal{H}(\mathbf{MA}(\Omega)|\mathbf{MA}(\Omega')) &= \frac{3\sqrt{3}}{\sqrt{2}\sqrt{k}} \cdot \sqrt{\epsilon} + o(\sqrt{\epsilon}), \\ \mathcal{H}(\mathbf{MAT}(\Omega)|\mathbf{MAT}(\Omega')) &= \frac{3\sqrt{3}}{\sqrt{k}} \cdot \sqrt{\epsilon} + o(\sqrt{\epsilon}), \end{aligned}$$

where $\epsilon = \max \{ \mathcal{H}(\Omega, \Omega'), \mathcal{H}(\partial\Omega, \partial\Omega') \} = \mathcal{H}(\partial\Omega, \partial\Omega')$.

7 Applications

We consider the special case when $\partial\Omega$ consists of quadratic splines. Assume that Ω is not weakly injective, and $\mathbf{MAT}(\Omega)$ does not contain a non-degenerate 1-prong point of the type (iii). Let P be a non-degenerate 1-prong point of $\mathbf{MAT}(\Omega)$. From the fact that $\partial\Omega$ is piecewise quadratic splines, it is easy to see that $A_3 = 0$, $A_4 = \frac{k_P^3}{8}$, and $N_P = 3$. See Examples 1, 4. From this observation and from Proposition 3, we have:

Corollary 1. Let Ω be a normal domain which is not weakly injective, and whose boundary consists of piecewise quadratic splines. Suppose $\mathbf{MAT}(\Omega)$ does not have a non-degenerate 1-prong point of type (iii). Then we have

$$\begin{aligned} \mathcal{H}(\mathbf{MA}(\Omega)|\mathbf{MA}(\Omega')) &\leq \frac{9\sqrt{2}}{\sqrt{k_\Omega}} \cdot \sqrt{\epsilon} + o(\sqrt{\epsilon}), \\ \mathcal{H}(\mathbf{MAT}(\Omega)|\mathbf{MAT}(\Omega')) &\leq \frac{9\sqrt{2}}{\sqrt{k_\Omega}} \cdot \sqrt{\epsilon} + o(\sqrt{\epsilon}), \end{aligned}$$

for any normal domain Ω' with $\min \{ \mathcal{H}(\Omega, \Omega'), \mathcal{H}(\partial\Omega, \partial\Omega') \} \leq \epsilon$, where

$$k_\Omega = \min \{ k_P : P \text{ is a non-degenerate 1-prong point of } \mathbf{MAT}(\Omega) \}.$$

To illustrate the above Corollary, let Ω' be the domain as depicted in Figure 10.

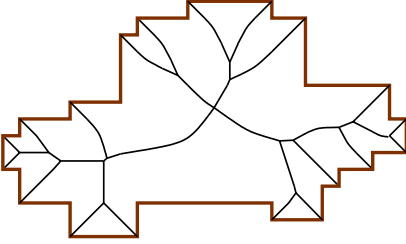


Figure 10: Original domain Ω' with its MA : $\mathbf{MA}(\Omega')$ and $\mathbf{MAT}(\Omega')$ have many unnecessary branches.

We approximate Ω' with a domain Ω which satisfies the assumptions in Corollary 1. Let $\epsilon = \max \{ \mathcal{H}(\Omega, \Omega'), \mathcal{H}(\partial\Omega, \partial\Omega') \} = \mathcal{H}(\partial\Omega, \partial\Omega')$. See Figure 11. Here, we have $k_\Omega = \frac{1}{R}$. So by Corollary 1, we have the following *a priori* estimates:

$$\begin{aligned} \mathcal{H}(\mathbf{MA}(\Omega)|\mathbf{MA}(\Omega')) &\leq 9\sqrt{2}\sqrt{R} \cdot \sqrt{\epsilon} + o(\sqrt{\epsilon}), \end{aligned} \quad (2)$$

$$\begin{aligned} \mathcal{H}(\mathbf{MAT}(\Omega)|\mathbf{MAT}(\Omega')) &\leq 9\sqrt{2}\sqrt{R} \cdot \sqrt{\epsilon} + o(\sqrt{\epsilon}). \end{aligned} \quad (3)$$

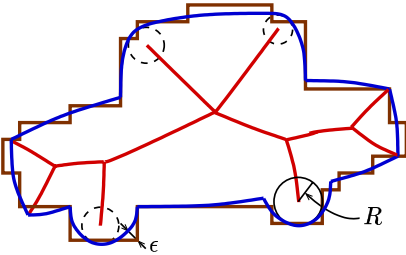


Figure 11: Approximation of the original domain Ω' by Ω whose boundary consists of piecewise quadratic splines: $\mathbf{MA}(\Omega)$ and $\mathbf{MAT}(\Omega)$ have much simpler forms.

See Figure 12 to compare $\mathbf{MA}(\Omega)$ and $\mathbf{MA}(\Omega')$. Note that $\mathbf{MA}(\Omega)$ reduces the complexity of $\mathbf{MA}(\Omega')$, while remaining roughly inside of $\mathbf{MA}(\Omega')$.

From (2) and (3), we can see that the one-sided Hausdorff distances $\mathcal{H}(\mathbf{MA}(\Omega)|\mathbf{MA}(\Omega'))$ and

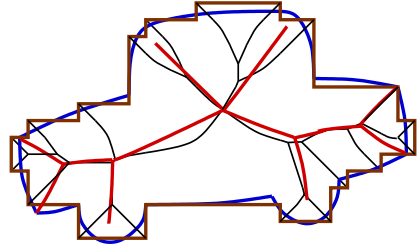


Figure 12: Comparison of the original MA and the approximated MA: The one-sided Hausdorff distance of $\mathbf{MA}(\Omega)$ with respect to $\mathbf{MA}(\Omega')$ is relatively small, while $\mathbf{MA}(\Omega)$ much simplifies $\mathbf{MA}(\Omega')$.

$\mathcal{H}(\mathbf{MAT}(\Omega)|\mathbf{MAT}(\Omega'))$ become smaller, when we shrink R and ϵ . This means that $\mathbf{MA}(\Omega)$ and $\mathbf{MAT}(\Omega)$ approximate $\mathbf{MA}(\Omega')$ and $\mathbf{MAT}(\Omega')$ more faithfully as we grow the maximum curvatures of the approximating domain Ω .

Another important observation is that we don't need to compute the whole MA and MAT to obtain the bounds (2) and (3), which was the case for the weakly injective domains [9]. It is sufficient to examine the boundary of the approximating domain Ω for the maximum curvatures.

We observed that the $\mathbf{MA}(\Omega)$ (and $\mathbf{MAT}(\Omega)$) is simpler than $\mathbf{MA}(\Omega')$ (and $\mathbf{MAT}(\Omega')$). The following Corollary tells that, even though $\mathbf{MA}(\Omega)$ (and $\mathbf{MAT}(\Omega)$) has fewer parts than $\mathbf{MA}(\Omega')$ (and $\mathbf{MAT}(\Omega')$), it nevertheless contains an essential part.

Corollary 2. *Let Ω' be a normal domain, and let Ω_1, Ω_2 be normal domains satisfying the assumptions in Corollary 1. Suppose $\max \{ \mathcal{H}(\Omega_i, \Omega'), \mathcal{H}(\partial\Omega_i, \partial\Omega') \} \leq \epsilon$ for $i = 1, 2$. Then we have*

$$\begin{aligned} \mathcal{H}(\mathbf{MA}(\Omega_1), \mathbf{MA}(\Omega_2)) &\leq \frac{18}{\sqrt{k}} \cdot \sqrt{\epsilon} + o(\sqrt{\epsilon}), \end{aligned}$$

$$\begin{aligned} \mathcal{H}(\mathbf{MA}(\Omega_1), \mathbf{MA}(\Omega_2)) &\leq \frac{18}{\sqrt{k}} \cdot \sqrt{\epsilon} + o(\sqrt{\epsilon}), \end{aligned}$$

where $k = \max \{ k_{\Omega_1}, k_{\Omega_2} \}$.

Proof. This follows by applying Corollary 1 symmetrically to Ω_1 and Ω_2 , and from the fact that

$$\begin{aligned} \mathcal{H}(\Omega_1, \Omega_2) &\leq \mathcal{H}(\Omega_1, \Omega) + \mathcal{H}(\Omega_2, \Omega) \leq 2\epsilon, \\ \mathcal{H}(\partial\Omega_1, \partial\Omega_2) &\leq \mathcal{H}(\partial\Omega_1, \partial\Omega) + \mathcal{H}(\partial\Omega_2, \partial\Omega) \leq 2\epsilon. \quad \square \end{aligned}$$

Note that the above bounds are for the two-sided Hausdorff distances instead of the one-sided ones. Thus, if we choose another approximation with the similar k_Ω , its MA and MAT are guaranteed to be approximately the same with the first approximation. This means that these approximations contain roughly the common parts of the original MA and MAT, whose degrees of the detail depend on the constant k_Ω and ϵ .

8 Conclusions

We have reviewed the results to bound the one-sided Hausdorff distance of the MAT with respect to the perturbed MAT, and illustrated them with some examples. We then applied them to pruning of the MAT with *a priori* error guarantees. For the weakly injective domains, we have linear bounds, but whose coefficients depend on the MAT. Though the linearity of the bounds is slightly violated, the domains which are not weakly injective have the coefficients which depend directly on the boundaries, which is a significant advantage over the weakly injective case.

References

[1] J. August, K. Siddiqi and S. W. Zucker, "Ligature instabilities and the perceptual organization of shape," *Computer Vision and Image Understanding*, vol. 76, no. 3, pp. 231–243, Dec. 1999.

[2] J. August, A. Tannenbaum and S. Zucker, "On the evolution of the skeleton," *Proc. 7th ICCV*, (Kerkyra, Greece), pp. 315–322, Sept. 1999.

[3] T. F. Banchoff and P. J. Giblin, "Global theorems for symmetry sets of smooth curves and polygons in the plane," *Proceedings of the Royal Society of Edinburgh*, vol. 106A, pp. 221–231, 1987.

[4] H. Blum, "A transformation for extracting new descriptors of shape," *Proc. Symp. Models for the Perception of Speech and Visual Form* (W.W. Dunn, ed.), MIT Press, Cambridge, MA, pp. 362–380, 1967.

[5] H. I. Choi, S. W. Choi and H. P. Moon, "Mathematical theory of medial axis transform," *Pacific J. Math.*, vol. 181, no. 1, pp. 57–88, Nov. 1997.

[6] H. I. Choi, C. Y. Han and J.-H. Yoon, "Medial axis transform distance and its applications," *Geometric Modeling and Computer Graphics 2000*, pp. 65–69, Kyung Moon Publisher, Seoul, Korea, April, 2000.

[7] S. W. Choi and S.-W. Lee, "Stability analysis of medial axis transform," *Proc. 15th ICPR*, (Barcelona, Spain), vol 3, pp. 139–142, Sept. 2000.

[8] S. W. Choi and H.-P. Seidel, "Hyperbolic Hausdorff distance for medial axis transform," Research Report, MPI-I-2000-4-003, 2000.

[9] S. W. Choi and H.-P. Seidel, "One-sided stability of medial axis transform," *Proceedings of Pattern Recognition, 23rd DAGM Symposium*, (Munich, Germany), Sept., 2001.

[10] S. W. Choi and H.-P. Seidel, "Medial axis transform is one-sidedly stable," *preprint*, 2001.

[11] M. P. Deseilligny, G. Stamon and C. Y. Suen, "Veinerization: A new shape descriptor for flexible skeletonization," *IEEE Trans. PAMI*, vol. 20, no. 5, pp. 505–521, May 1998.

[12] P. J. Giblin and B. B. Kimia, "On the local form and transitions of symmetry sets, medial axes, and shocks," *Proc. 7th ICCV*, (Kerkyra, Greece), pp. 385–391, Sept. 1999.

[13] V. Guillemin and A. Pollack, *Differential Topology*, Prentice-Hall, Inc., 1974.

[14] F. Mokhtarian and A. K. Mackworth, "A theory of multiscale, curvature-based shape representation for planar curves," *IEEE Trans. PAMI*, vol. 14, no. 8, pp. 789–805, Aug. 1992.

[15] U. Montanari, "A method for obtaining skeletons using a quasi-Euclidean distance," *J. of the ACM*, vol. 18, pp. 600–624, 1968.

[16] J. Serra, *Image analysis and mathematical morphology*, Academic Press, 1984.

[17] D. Shaked and A. M. Bruckstein, "Pruning medial axes," *Computer Vision and Image Understanding*, vol. 69, no. 2, pp. 156–169, Feb. 1998.